Journal of Alloys and Compounds 523 (2012) 161–166

Contents lists available at SciVerse ScienceDirect

Journal of Alloys and Compounds

journal homepage: www.elsevier.com/locate/jallcom

Solvothermal synthesis and upconversion spectroscopy of monophase hexagonal $NaYF_4:Yb^{3+}/Er^{3+}$ nanosized crystallines

Jing Guo, Feizhong Ma, Shuangna Gu, Ying Shi*, Jianjun Xie

Department of Electronics and Information Materials, School of Material Science and Engineering, Shanghai University, Shanghai 200072, PR China

ARTICLE INFO

Article history:
Received 7 September 2011
Received in revised form 19 January 2012
Accepted 24 January 2012
Available online 2 February 2012

Keywords:
$NaYF_4$:Yb/Er
Solvothermal synthesis
Hexagonal
Upconversion

ABSTRACT

The synthesis of single-phase hexagonal $NaYF_4:Yb^{3+}/Er^{3+}$ upconversion phosphors was investigated by a facile solvothermal processing. It was found that solvents adopted could influence the phase composition, morphology and luminescence property of resultant $NaYF_4$ nanosized crystals greatly. When a mixture of oleic acid–glycol–ethanol was used as solvent, the monophase hexagonal $NaYF_4:Yb^{3+}/Er^{3+}$ nanocrystals were successfully obtained, which exhibited nanorods morphology with a longitude of about 200 nm and a diameter of 50–80 nm. By co-doping Yb^{3+} and Er^{3+}, hexagonal $NaYF_4$ nanorods emitted bright upconversion luminescence at 530 nm and 652 nm under excitation of 980 nm, which was much superior than those of $NaYF_4:Yb^{3+}/Er^{3+}$ particles synthesized in other solvents such as deionized water, ethanol, glycol and oleic acid.

1. Introduction

Upconversion (UC) luminescent materials have numerous potential applications in solid-state lasers [1,2], solar cells [3,4], infrared photodetectors [5], three-dimensional displays [6–8] and biological labels [9–11]. Compared with organic dyes, quantum dots and metallic nanoparticles [12,13], UC inorganic fluorescent nano-materials possess many special advantages in the area of biological labeling, such as the absence of auto-fluorescence, reduced light scattering, greater luminescence penetration depths and high resistance of photobleaching. Hexagonal phase sodium yttrium tetrafluoride (β-$NaYF_4$) has been reported as one of the most efficient hosts which contribute to convert 980 nm NIR to visible light. By co-doping Yb^{3+}/Er^{3+}, the hexagonal phase $NaYF_4:Yb^{3+}/Er^{3+}$ can emit bright green luminescence, whose green emission intensity is 10 times stronger and overall (green-plus-red) emissions are 4.4-times greater than those for the cubic phase $NaYF_4$ [14]. So the key point is that how to synthesis pure hexagonal phase $NaYF_4:Yb^{3+}/Er^{3+}$ with high luminous intensity by facile routes.

Recently, several methods have been developed to synthesize $NaYF_4$ aiming to obtain single-phase hexagonal $NaYF_4$ particles with desirable chemical compositions and controllable microstructure, such as one-step synthesis [15], solvothermal processing [16–18], co-precipitation method [19,20], microwave-assisted synthesis [21,22] and thermolysis processing [23]. Among them, solvothermal method is a kind of ideal way to synthesize nanosized materials. Reaction temperatures, heat treatment time, pH value of solution, precursor concentration, slovents and compaction rate are important factors to control the phase, morphology and property of the obtained crystals [24]. A solvothermal strategy to prepare $NaLaF_4$ nanorods in water–ethanol–oleic acid mixing system has been proposed by Wang et al. [25]. Chen et al. [26] have reported a solvothermal synthesis of $NaYF_4$:Yb/Er nano-structured materials with controlled shapes by tuning the solvents, such as ethylene glycol and polyethylene glycol, nevertheless monophase β-$NaYF_4$ was not obtained. Hua and coworkers [27] found that hexagonal phase $NaYF_4:Yb^{3+}/Er^{3+}$ microtubes could be synthesized through a hydrothermal processing by using YF_3 sub-microspindles as precursor. Therefore, it is feasible to take advantage of solvothermal method for synthesizing hexagonal phase $NaYF_4:Yb^{3+}/Er^{3+}$ with uniform dispersed state and high luminescence intensity.

In this paper, we presented a solvothermal approach to achieve simultaneous control over the crystallographic phase, morphology and luminescence intensity of β-$NaYF_4$ by just choosing appropriate solvents. Oleic acid (OA)–glycol–ethanol, oleic acid, glycol, ethanol and water were chosen as solvents, respectively. Single-phase β-$NaYF_4:Yb^{3+}/Er^{3+}$ nanocrystals were synthesized successfully by tuning the solvents. The upconversion emission properties of resultant $NaYF_4$ nanocrystals were also characterized.

2. Experimental procedures

2.1. Preparation of $NaYF_4$ nanorods

All chemicals were of analytical grade and used as received. In a typical procedure of the preparation of $NaYF_4$:20%Yb^{3+}/2%Er^{3+}, 0.24 g of Y_2O_3, 0.096 g of Yb_2O_3

* Corresponding author. Tel.: +86 021 56332574; fax: +86 021 56332694.
E-mail address: yshi@shu.edu.cn (Y. Shi).

0925-8388/$ – see front matter © 2012 Elsevier B.V. All rights reserved.
doi:10.1016/j.jallcom.2012.01.135

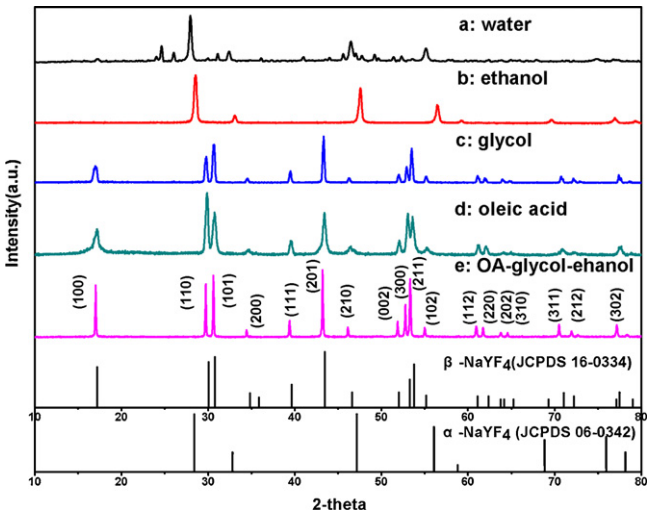

Fig. 1. X-ray powder diffraction patterns of as-prepared $NaYF_4$:Yb^{3+}/Er^{3+} by solvothermal processing in (a) water, (b) ethanol, (c) glycol, (d) oleic acid and (e) oleic acid–glycol–ethanol.

and 0.01 g of Er_2O_3 were dissolved in a concentrated HNO_3 acid, and then evaporated to dryness in oven at 80 °C. After 25 ml glycol was added, the mixture was stirred by magnetic stirrers to form transparent solution. Afterwards, 15 ml oleic acid, 10 ml ethanol, 0.8 g NH_4F and 2.0 g C_2H_5ONa were mixed into the solution. After being agitated at 80 °C for 30 min, the solution was transferred into a teflon vessel (100 ml). After autoclave was tightly sealed, the teflon vessel was placed into a stainless steel kettle to undertake a solvothermal processing at 200 °C for 24 h. The obtained products (sample e) in teflon vessel were washed 5 times with deionized water and absolute ethanol respectively in turn, followed by being dried in air at 80 °C for 12 h. As comparison, the second sample (sample a) was prepared in 50 ml pure water under the same reaction conditions, the third one (sample b) was in 50 ml pure ethanol, the fourth one (sample c) was in 50 ml glycol and the last one (sample d) was in 50 ml OA, respectively.

2.2. Characterization

X-ray diffraction (XRD) measurements of samples a–d were performed in order to determine the phase composition of products on a Rigaku Dmax-2550 X-ray diffractometer with Cu Kα-radiation resource (λ = 1.5406 Å). To determine the purity of sample e, X-ray diffraction (XRD) measurement was performed by using synchrotron light source (λ = 1.2398 Å) in BL14B1 line station of Shanghai Synchrotron Radiation Facility. The data obtained could be transformed to fit the requirement of JCPDS cards by using wavelength-transformation software. The morphologies of products were recorded by field emission electron microscope (FE-SEM, JSM-6700F). The transmission electron microscope (TEM) and selected area electron diffraction (SAED) patterns were characterized by transmission electron microscope

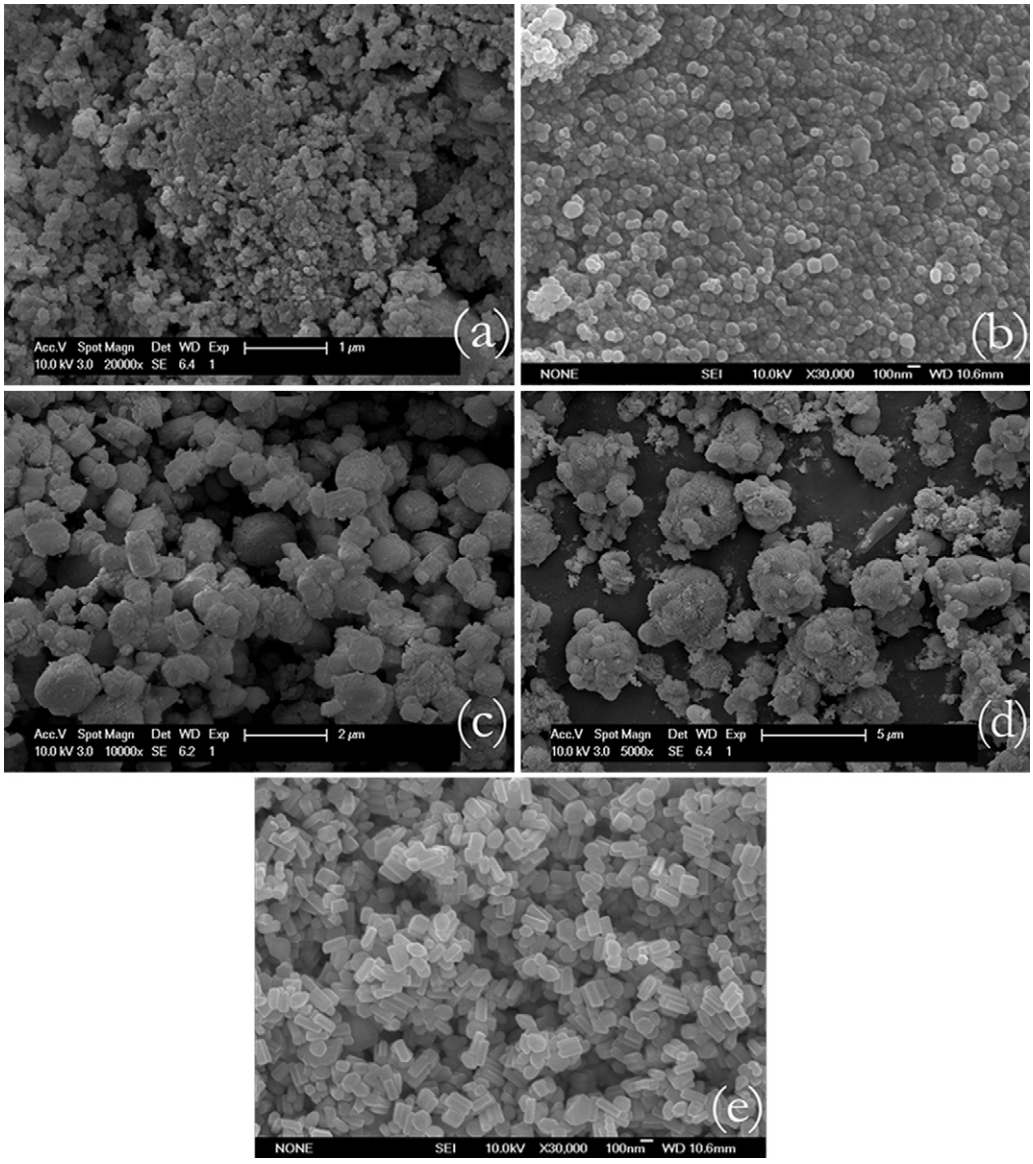

Fig. 2. SEM images of the $NaYF_4$:Yb^{3+}/Er^{3+} nanosized particles obtained in (a) water, (b) ethanol, (c) glycol, (d) oleic acid and (e) oleic acid–glycol–ethanol.

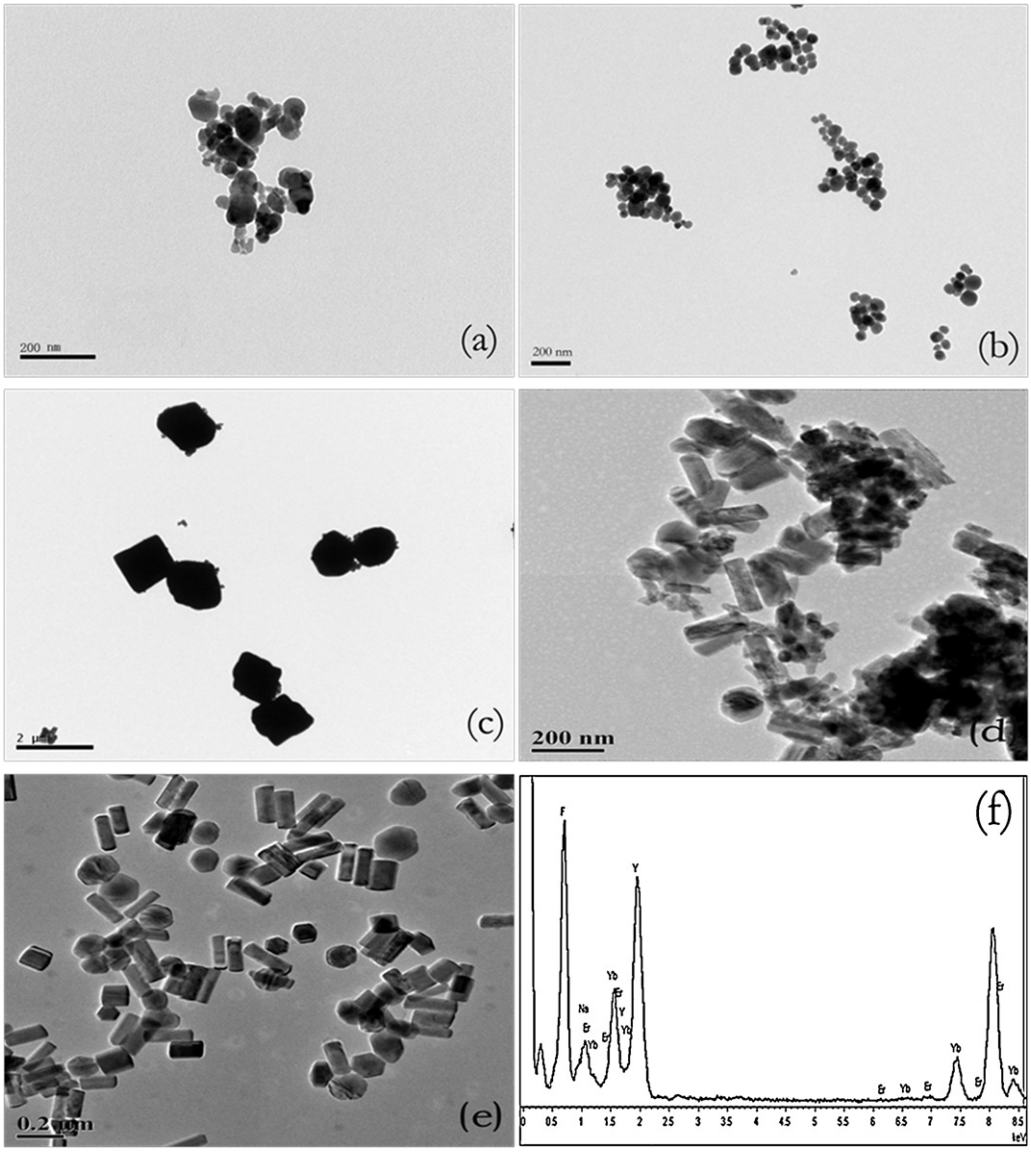

Fig. 3. TEM images of the $NaYF_4$:Yb^{3+}/Er^{3+} nanocrystals synthesized in (a) water, (b) ethanol, (c) glycol, (d) oleic acid and (e) oleic acid–glycol–ethanol. (f) Typical EDX pattern of the above $NaYF_4$:Yb^{3+}/Er^{3+} nanocrystals.

(JEM-2010F). The upconversion emission spectras were measured by Fluorolog-3 fluorescence spectrometer (Jobin Yvon, France) using 980 nm laser as the excitation source. All the measurements were performed under room temperature.

3. Results and discussion

3.1. Effect of solvents on phase composition of $NaYF_4$

The phase compositions of the solvothermal products were firstly examined by X-ray diffraction (XRD). Fig. 1 showed the XRD patterns of the as-prepared $NaYF_4$:Yb^{3+}/Er^{3+} products. The diffractive peaks in curve 1a for sample (a) could be mainly indexed to $Na_{1.5}Y_{2.5}F_9$ (JCPDS 39-0723). All diffraction peaks of the cubic phase $NaYF_4$ (α-$NaYF_4$) observed in sample b were in good agreement with the data in JCPDS 06-0342 (pattern b of Fig. 1). Samples c–e exhibited the peaks of hexagonal $NaYF_4$, which were consistent with the literature data (JCPDS 16-0334) quite well. The sharp diffraction peaks proved that the obtained products were well crystallized. It was suggested that glycol, OA and OA–glycol–ethanol were capable of accelerating the formation of single-phase β-$NaYF_4$ under relative lower temperatures. No second phase was detected in the XRD measurements, indicating that Er^{3+}, Yb^{3+} ions were effectively doped into the host lattice of β-$NaYF_4$. As shown in Table 1, the solvent viscosity of oleic acid was highest among these solvents the reasonable explanation could be presumed that high value of solvent viscosity might play an important role in dominating the formation of hexagonal $NaYF_4$ nanocrystals. When the $NaYF_4$:Yb^{3+}/Er^{3+} nanocrystals were synthesized in pure oleic acid, the sample tended to be contaminated for the decomposition of oleic acid. As a result, the color of obtained powder turned gray or black. Considering that the oleic acid has a good dissolubility in ethanol, and the existence of glycol facilitates the fabrication of β-$NaYF_4$, it could be argued that the mixture of oleic acid–glycol–ethanol was a desirable combination for the synthesis of pure β-$NaYF_4$ under solvothermal conditions.

Table 1
The viscosity value of solvents used at 20 °C.

Solvent	Water	Ethanol	Glycol	Oleic acid
Viscosity (20 °C)/mPa s	1.0050	1.200	19.9	25.6 (30 °C)

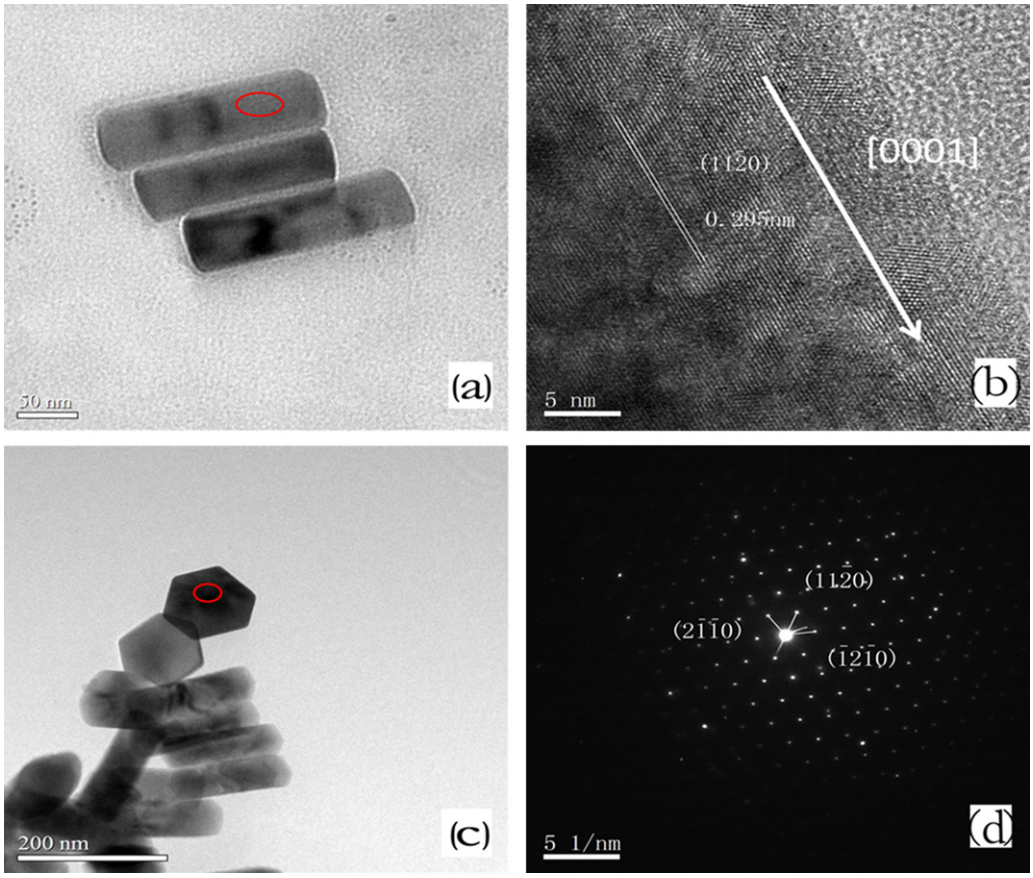

Fig. 4. (a) TEM images of hexagonal β-$NaYF_4$:Yb^{3+}/Er^{3+} nanorods (side of the rod). (b) HRTEM image of $NaYF_4$:Yb^{3+}/Er^{3+} nanorods (standing on the side face) in OA–glycol–ethanol. (c) TEM image of $NaYF_4$:Yb^{3+}/Er^{3+} nanorods (top of the rod). (d) SAED pattern of $NaYF_4$:Yb^{3+}/Er^{3+} nanorods (standing on the top side face) in oleic acid–glycol–ethanol.

3.2. The morphology variation of $NaYF_4$ on solvents used

Fig. 2 showed morphology variation of β-$NaYF_4$:Yb^{3+}/Er^{3+} nanosized crystals depening on solvents adopted in the course of solvothermal processing. The SEM image of sample a (Fig. 2(a)) obtained in pure water displayed that the nanocrystals consisted of irregular globular particles with the size around 50 nm. However, while the solvent was changed to ethanol, significant change in phase and morphology of $NaYF_4$ particles occurred. The image of sample b (Fig. 2(b)) demonstrated that the obtained α-$NaYF_4$ particles were in spherical shape with the diameter of 50–100 nm. From the SEM image of the sample c (Fig. 2(c)) synthesized in glycol, it was revealed that the products had morphology of hexagonal microplates with an average diameter of 500 nm to 1 μm and a thickness of 500 nm. Meanwhile, the edges of the plates were rough. A small quantity of single $NaYF_4$ nanorods obtained in OA could be observed in Fig. 2(d), in which most crystals existed in agglomerate state. As shown in Fig. 2(e), β-$NaYF_4$ nanocrystals obtained in oleic acid–glycol–ethanol mixture grew into regular anisotropic nanorods structures with an average length of 150–200 nm and a diameter of 60–80 nm.

Fig. 3 displayed TEM images of the as-synthesized $NaYF_4$ nanocrystals in different solution environment. The products obtained in water and ethanol (Fig. 3(a) and (b)) displayed a spherical morphology with particle size of ~50 nm. Fig. 3(c) showed square and round β-$NaYF_4$ synthesized in glycol, with the diameter of 1–2 μm. In this case, β-$NaYF_4$ crystals were in micrometer scale and difficult to meet the requirements of practical applications. As glycol was changed for OA, β-$NaYF_4$ nanorods were formed substantially with a typical length of ~200 nm, which was clearly shown in Fig. 3(d). The TEM image shown in Fig. 3(e) demonstrated that the β-$NaYF_4$ nanocrystals obtained in oleic acid–glycol–ethanol mixture were of single-crystal nature. All β-phase $NaYF_4$ (Fig. 3(e)) nanorods were of hexagonal nanocrystal nature with a uniform size of about 50–80 nm in diameter and 200 nm in length, which corresponded to result of Fig. 2(e). The EDX spectrum in Fig. 3(f) proved that Yb and Er were detected in all the products, demonstrating that the Yb^{3+} and Er^{3+} ions were introduced into $NaYF_4$ host lattice.

The typical HRTEM images and SAED patterns in Fig. 4(a)–(d) provided a further insight into the nanometer-scale structural details of the β-$NaYF_4$ nanorods (sample d). Some of the rods standed on the TEM grids via the side faces (Fig. 4(a)), while others existed on the TEM grids on their bottom faces, showing unambiguously high crystallinity and a regular hexagonal cross-section (Fig. 4(c)), which corresponded to hexagonal microprisms that were parallel and perpendicular to the copper grids, respectively. The HRTEM image in Fig. 4(b) showed an interplanar spacing of 0.295 nm corresponding to the (1 1 2 0) planes. Moreover, as disclosed by HRTEM images (Fig. 4(b)), the β-$NaYF_4$ nanorods exhibited a preferred growth direction along [0 0 0 1]. The SAD diffraction pattern (Fig. 4(d)) of hexagonal cross-section proved fully the single crystalline nature of $NaYF_4$:Yb^{3+}/Er^{3+} nanocrystals, whose zone axis was [0 0 0 1].

It was not cleat yet about the exact mechanism of the solvents effect on phase composition and particles morphology. Laudise' group [28] reported that the difference in the growth rates of various crystal facets was a key factor to determine the different morphologies of the crystallites. Mann [29] also claimed that the unit cell symmetry governed the spatial relations between the

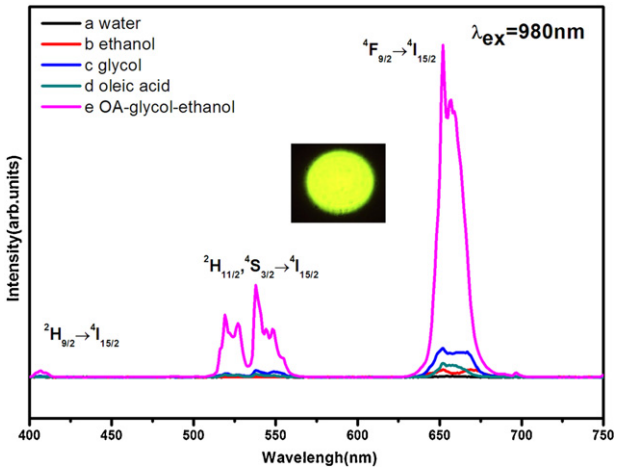

Fig. 5. Upconversion emission spectra of $NaYF_4$ nanoparticles synthesized in different solvents (Slit width: 0.8 nm, 28 MW). The inset picture is digital photograph of the total luminescence of sample e without using any filters.

facets. However, their selection was mechanistically determined by the relative rates of growth along different crystallographic directions. So a logical explanation could be proposed that the nanocrystals were inclined to have a harmonious growth rate for different crystal planes in the solvents with low value of viscosity. It seemed that the solvent viscosity was one of the important factors to determine the morphology of nanoparticles in solvothermal processing. As shown in Table 1, ions' diffusion rate was low in solvents with high viscosity, resulting in slower and less nucleation. As a result, the larger size of crystals were easier to be accessed. Meanwhile, organic molecules provided a template for crystal growth by binding with special crystal planes, leading to anisotropic crystal growth. In this experiment, it was inferred that the solvent viscosity and organic molecules played roles together to determine the size and morphology of obtained $NaYF_4$ crystals.

3.3. Upconversion luminescence of obtained $NaYF_4$ particles

In the process of upconversion, Yb^{3+} ions provided two energy transfers for the population of the excited states. After subsequent multiphonon relaxation, radiative emissions occurred. The NIR upconversion spectras of $NaYF_4$:Yb^{3+}/Er^{3+} synthesized in different solvents under 980 nm excitation (excitation power: 28 MW) were illustrated in Fig. 5. By doping Er^{3+} ions into the system, three characteristic emission peaks were observed, which corresponded to electron transition $^2H_{9/2}\rightarrow{}^4I_{15/2}$ (410 nm), $^2H_{11/2}$, $^4S_{3/2}\rightarrow{}^4I_{15/2}$ (525 and 540 nm), and $^4F_{9/2}\rightarrow{}^4I_{15/2}$ (660 nm), respectively. All of the spectras were similar to what had been reported for these materials [10,30,31]. The inset of Fig. 5 showed a digital photograph of the total upconversion luminescence of sample e taken under the excitation conditions by ordinary optical camera. The total light appeared yellow–green in color because of a stacking of red and green emissions from the Er^{3+} ions. The red emissions were significantly stronger than the green ones, which might result from the rapid $^4S_{3/2}\rightarrow{}^4F_{9/2}$ nonradiative decay that rendered the green level nonemissive [31]. And the radio of green to red depended also on the excitation power because the emitting states had different population mechanisms [14].

Upconversion efficiency mainly depended on the phase purity, as well as dopant concentration, ratio of Na to rare earth ions and preparation temperature [32]. It was also reported that the particle size and the organic capping groups binding on the surface of the $NaYF_4$ crystals could affect the emission intensity [33]. In this paper, combined with microstructural observation, it was suggested that oleic acid–glycol–ethanol mixture was a suitable solvent to synthesize $NaYF_4$:Yb^{3+}/Er^{3+} with high luminous intensity under mild conditions. $NaYF_4$:Yb^{3+}/Er^{3+} crystals with the same hexagonal structure had different capacities for upconversion luminescence, which was shown in Fig. 5(d) and (e). It could be explained as follows, the solvents with high viscosity value could contribute to crystallization of β-$NaYF_4$ nanorods, which led to the controllable morphology and high UC intensity [34].

4. Conclusions

Simultaneous control over the phase, morphology and luminescence intensity of $NaYF_4$ nanocrystals was realized in oleic acid–glycol–ethanol mixture by facile solvothermal synthesis. Pure hexagonal phase $NaYF_4$:20%Yb/2%Er nanocrystals with high luminous intensity were synthesized successfully in our experiment. Under optimized conditions the resultant β-$NaYF_4$ exhibited nanorods morphology with a length of 200 nm and a hexagon cross-section. It can be presumed that the oleic acid could help the formation of β-$NaYF_4$ nanorods along [0 0 0 1]. As a result, the strong upconversion emission peaks were achieved at wavelength of 530 nm and 650 nm under excitation of 980 nm.

Acknowledgements

This work was partly supported by Shanghai Leading Academic Disciplines (S30107). The authors gratefully acknowledge the Analysis and Testing Centre of Shanghai University and Shanghai Synchrotron Radiation Facility for technical support.

References

[1] P. Xie, T.R. Gosnell, Opt. Lett. 20 (1995) 1014–1016.
[2] M. Kwaśny, Z. Mierczyk, R. Stępień, K. Jędrzejewski, J. Alloys Compd. 300–301 (2000) 341–347.
[3] A. Shalav, B.S. Richards, T. Trupke, K.W. Kramer, H.U. Güdel, Appl. Phys. Lett. 86 (2005) 013505.
[4] D.C. Yu, X.Y. Huang, S. Ye, Q.Y. Zhang, J. Alloys Compd. (2011), doi:10.1016/j.jallcom.2011.07.088.
[5] C.J. Sun, Z.H. Xu, B. Hu, G.S. Yi, G.M. Chow, J. Shen, Appl. Phys. Lett. 91 (2007) 191113–191115.
[6] E. Downing, L. Hesselink, J. Ralston, R. Macfarlane, Science 273 (1996) 1185–1189.
[7] X.S. Qiao, X.P. Fan, Z. Xue, X.H. Xu, Q. Luo, J. Alloys Compd. 509 (2011) 4714–4721.
[8] W. Wang, J. Ren, D.P. Chen, S.L. Yuan, G.R. Chen, J. Alloys Compd. 516 (2012) 1–4.
[9] P. Zhang, S. Rogelj, K. Nguyen, D. Wheeler, J. Am. Chem. Soc. 128 (2006) 12410–12411.
[10] F. Wang, D. Banerjee, Y.S. Liu, X.Y. Chen, X.G. Liu, Analyst 135 (2010) 1839.
[11] F. Vetrone, R. Naccache, A. Zamarrón, A. Juarranz de la Fuente, F. Sanz-Rodríguez, L.M. Martinez, E.M. Rodriguez, D. Jaque, J.G. Solé, J.A. Capobianco, Nanoscale 4 (2010) 3254–3258.
[12] E.M. Sevick-Muraca, J.P. Houston, M. Gurfinkel, Curr. Opin. Chem. Biol. 6 (2002) 642–650.
[13] B.R. Masters, P.T.C. So, Handbook of Biomedical Nonlinear Optical Microscopy, Oxford University Press, Oxford, 2008.
[14] K.W. Kramer, D. Biner, G. Frei, H.U. Gudel, M.P. Hehlen, S.R. Luthi, Chem. Mater. 16 (2004) 1244–1251.
[15] M. Wang, C.C. Mi, J.L. Liu, X.L. Wu, Y.X. Zhang, W. Hou, F. Li, S.K. Xu, J. Alloys Compd. 485 (2009) L24–L27.
[16] G.F. Wang, W.P. Qin, J.S. Zhang, L.L. Wang, G.D. Wei, P.F. Zhu, R. Kim, J. Alloys Compd. 475 (2009) 452–455.
[17] S.J. Zeng, G.Z. Ren, C.F. Xu, J. Alloys Compd. 509 (2011) 2540–2543.
[18] S.J. Zeng, G.Z. Ren, Q.B. Yan, J. Alloys Compd. 493 (2010) 476–480.
[19] C.Y. Cao, X.M. Zhang, M.L. Chen, W.P. Qin, J.S. Zhang, J. Alloys Compd. 505 (2010) 6–10.
[20] G.S. Yi, H.C. Lu, S.Y. Zhao, Y. Ge, W.J. Yang, D.P. Chen, L.H. Guo, Nano Lett. 4 (2004) 2191–2196.
[21] X. Chen, W.J. Wang, X.Y. Chen, J.H. Bi, L. Wu, Z.H. Li, X.Z. Fu, Mater. Lett. 63 (2009) 1023–1026.
[22] L. Zhang, Y.J. Zhu, J. Inorg. Mater. 24 (2009) 553–558.
[23] J.N. Shan, Y.G. Ju, Appl. Phys. Lett. 91 (2007) 123103.
[24] K. Byrappa, T. Adschiri, Progr. Cryst. Growth Charact. Mater. 53 (2007) 117–166.
[25] L.Y. Wang, P. Li, Y.D. Li, Adv. Mater. 19 (2007) 3304–3307.

[26] Z.G. Chen, Q.W. Tian, Y.L. Song, J.M. Yang, J.Q. Hu, J. Alloys Compd. 506 (2010) L17–L21.
[27] Y. Tian, R.N. Hua, N.S. Yu, W. Zhang, L.Y. Na, B.J. Chen, J. Alloys Compd. (2011), doi:10.1016/j.jallcom.2011.07.095.
[28] R.A. Laudise, E.D. Kolb, A.J. Caporaso, J. Am. Chem. Soc. 47 (1964) 9–12.
[29] S. Mann, Angew. Chem. Int. Ed. 39 (2000) 3392–3406.
[30] J.C. Boyer, L.A. Cuccia, J.A. Capobianco, Nano Lett. 7 (2007) 847–852.
[31] R.H. Page, K.I. Schaffers, P.A. Waide, J.B. Tassano, S.A. Payne, W.F. Krupke, J. Opt. Soc. Am. B 15 (1998) 996–1008.
[32] J.F. Suyver, A. Aebischer, D. Biner, P. Gerner, J. Grimm, S. Heer, K.W. Kräme, C. Reinhard, H.U. Güdel, Opt. Mater. 27 (2005) 1111–1130.
[33] Y. Wei, F.Q. Lu, X.R. Zhang, D.P. Chen, Chem. Mater. 18 (2006) 5733–5737.
[34] X.C. Jiang, L.D. Sun, W. Feng, C.H. Yan, Cryst. Growth Des. 4 (2004) 517–520.